Optically induced spin echoes in rubidium atoms: On- and off-resonant manipulations of spins

T. Moriyasu,[1] Y. Koyama,[2] Y. Fukuda,[1] and T. Kohmoto[2]
[1]*Graduate School of Science and Technology, Kobe University, Kobe 657-8501, Japan*
[2]*Graduate School of Science, Kobe University, Kobe 657-8501, Japan*
(Received 12 January 2008; revised manuscript received 22 April 2008; published 1 July 2008)

We studied the optical manipulation of spin coherence in rubidium atoms by using polarization spectroscopy with the pump-probe technique. Two types of optically induced spin echoes, namely on- and off-resonant manipulations, whose creation mechanism are the optical pumping effect and the light shift effect, respectively, are studied theoretically and experimentally. A theory of optically induced spin echoes that can be applied to both types of spin echoes is considered by using the density matrix, and a general expression for the refocusing efficiency of the control pulse is presented. The effect of the off-resonant manipulation was examined by using light pulses of two frequencies provided by two lasers. Vector models for the two types of spin echoes are presented, and the observed dependences of the frequency and the duration of the control pulse on the spin-echo intensity are suitably explained by the theoretically derived refocusing efficiency. The off-resonant manipulation gives the possibility of arbitrary-angle spin rotation around an arbitrary axis.

DOI: 10.1103/PhysRevA.78.013402 PACS number(s): 42.50.Md, 32.60.+i

I. INTRODUCTION

Over the last decade, there has been significant interest in quantum-information processing. Among the broad range of approaches currently being investigated in this field, important progress has been achieved with trapped ions and atoms [1,2]. Entanglement and quantum gate operations have been realized [3–6]. An array of atoms can serve as a register of atomic qubits [7,8]. Each trap can act as a memory site for quantum information encoded in the two substates in the ground states of the atoms, which can be modeled as a collection of spin-1/2 particles [9]. In trapped-atom systems, the optical manipulation of spins plays very important roles. Many theoretical and experimental proposals and demonstrations for the realization of quantum-information processing using trapped atoms have been reported, such as quantum entanglement using trapped atomic spins [10], absorption-free optical control of spin systems [11], quantum-limited measurement [12], generation of a superposition of spin states in an atomic ensemble [13], geometric two ion-qubit phase gates [14] and error-resistant distributed quantum computation [15], high-efficiency spin state measurements [16], freezing distributed entanglement and controlled propagation of quantum information in spin chains [17], and initialization and readout of a qubit in an optical tweezer [18]. The optical manipulation of spins is essential for the implementation of these types of quantum processing. For solid-state hosts, room-temperature controlled coupling and universal two-qubit gates for vacancy centers in diamond have been discussed [19,20].

The optical manipulation of spins is also important for verifying the nonadiabatic quantum phases in electron spin systems [21]. The geometric phases, adiabatic Berry phase [22] and nonadiabatic Aharonov-Anandan phase [23], are of fundamental interest in physics. Their existence has been experimentally demonstrated in many physical systems such as molecules [24], light polarization in fibers [25], nuclear magnetic resonance (NMR) [26–28], and neutron polarization [29].

Recently, quantum computing in spin systems has been demonstrated by manipulating nuclear spins using the NMR technique [30,31]. If the spin can be manipulated voluntarily by an all-optical method, more rapid control of the spin system can be realized. Spin manipulation by optical pulses can provide broadband responses as compared to that by NMR or electron spin resonance (ESR). If we use ultrashort laser pulses, observations of ultrafast spin dynamics in the gigahertz and terahertz regions can be realized [32]. Several studies have demonstrated the ultrafast optical manipulation of spins, for example, ultrafast coherent spin rotation and phase control in ferromagnetic films [33], semiconductor quantum wells [34], and quantum dots [35,36], reliable precessional magnetization reversal in micrometer-sized elliptical permalloy elements [37], femtosecond photomagnetic switching of spins in ferrimagnetic films [38], ultrafast coherent spin control and magnetic recording with circularly polarized light in an amorphous ferrimagnetic metal [39,40], and zero-field optical manipulation of diluted spins in semiconductor quantum wells [41].

Coherent transient phenomena in sublevel systems, such as free induction decay (FID) and spin echoes, have been widely studied and used in the magnetic-resonance spectroscopy. These signals are generated by the coherent spin rotation, which is a fundamental spin manipulation, using pulsed radio-frequency (rf) or microwave fields. Coherent transients in sublevel systems can also be induced by light pulses. Sublevel echoes can be produced by optical spin manipulations without any use of rf or microwave pulses. In optically induced spin echoes, the coherence is not only generated by a light pulse but is also detected by a light pulse.

Sublevel coherence is induced by the first excitation pulse at $t=0$; however, the induced FID signal dephases due to the inhomogeneous distribution of the sublevel splittings. The second excitation pulse at $t=\tau$ refocuses the dephased coherence as an optically induced spin echo at $t=2\tau$, which is similar to the spin echoes in magnetic resonance techniques such as NMR and ESR. Photon echoes [42,43] are the optical analog of the spin echoes, where the frequency of the relevant two-level systems is extended from the radio or mi-

crowave frequency to the optical frequency. However, they have no direct applications to spin manipulation.

The studies of optically induced spin echoes for on-resonant [44] and off-resonant [45] manipulations have been performed independently. According to the theory of the on-resonant manipulation, the optically induced spin echoes are created by the optical pumping effect of resonant excitation pulse, and the effect of detuned excitation pulse is not considered. According to the theory of the off-resonant manipulation, on the other hand, the spin echoes are created by the light shift effect, and the optical pumping effect is not considered. In an experiment on the on-resonant manipulation [44], the laser frequency was tuned to the resonance line. In an experiment on the off-resonant manipulation in sodium atoms [45], the frequencies of the first and second excitation pulses and the probe light, which were provided by a single laser, were the same, and they were swept simultaneously. Since the generation and probe efficiencies of the sublevel coherence are changed under such an experimental condition, correct frequency dependence of the refocusing efficiency for the off-resonant manipulation is not necessarily obtained. Thus far, no theory that is valid for both types of optically induced spin echoes has been proposed, and no strict experiments on the spin echoes in off-resonant manipulation, where the refocusing efficiency of the excitation pulse is examined under the constant generation and probe efficiencies of the sublevel coherence, have been performed.

In the present study, optically induced spin echoes, which have potential applications in the quantum-information processing, optical control of geometric phases, and ultrafast coherent manipulation of spins, are studied theoretically and experimentally. Both types of spin echoes, on- and off-resonant manipulations, are considered from the viewpoint of spin manipulation. We consider a theory for optically induced spin echoes by using the density matrix, which can be applied to both on- and off-resonant manipulations, and a general expression for the refocusing efficiency of the control pulse is derived. The optically induced FID and spin echoes in rubidium atoms were observed by using polarization spectroscopy with the pump-probe technique. Two types of spin echoes, on- and off-resonant manipulations, were observed, where light pulses of two frequencies were provided by two independent lasers and were used to examine the effect of the off-resonant manipulation. We provide vector models for the two types of spin echoes, and the observed frequency and pulse-duration dependences of the refocusing efficiency are compared with the result of the theory. We show the possibility of arbitrary-angle spin rotation around an arbitrary axis using the off-resonant manipulation.

II. THEORY OF OPTICALLY INDUCED SPIN ECHOES

The optically induced spin echoes can be produced by the all-optical manipulation of spins. The spin-echo signal appears at $t=2\tau$ when the first and second pulses are applied at $t=0$ and τ. Since the first pulse generates the magnetization and the second pulse controls the magnetization generated by the first pulse, we refer to the first and second pulses as the generation and control pulses, respectively.

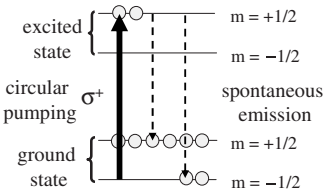

FIG. 1. Diagram of the four-level system. The solid arrow indicates the transition by the σ^+ circular pumping, and the broken arrows indicate the transitions by the spontaneous emission.

Using the simple four-level system shown in Fig. 1, we consider the effect of the generation pulse.

The σ^+ circular pumping increases the magnetic quantum number by one on the optical transition under the angular-momentum conservation. In the system treated here, the lifetime of the atoms in the excited state is very short. Therefore, a large population difference is generated in the ground state. This is the magnetization in the direction of the laser beam.

With regard to the effect of the control pulse, we consider two cases, where the frequency of the control pulse is on-resonance and off-resonance to the absorption lines of the atoms. Spin-echo signals appear in both cases. However, the echoes are created by different mechanisms in each case. The creation mechanism in on-resonant manipulation is the optical pumping, while that in off-resonant manipulation is the light shift.

The theories of the spin echoes for the on-resonant [44] and off-resonant [45] manipulations were developed independently. For the on-resonant manipulation, the detuning is ignored. For the off-resonant manipulation, on the other hand, the damping effect of the optical pumping is considered, but the contribution to the spin-echo signal from the optical pumping is ignored. Here, we consider a theory for the optically induced spin echoes by using the density matrix, which includes the detuning effect and can be applied to both the on- and off-resonant manipulations.

We consider the time evolution of the sublevel coherence generated from a set of a large number of atoms whose sublevel splittings are inhomogeneously distributed. A macroscopic signal, FID, created by the generation pulse does not persist for a long time because each atom develops at its own frequency even if the sublevel coherence of each atom is sustained for a long time. The optically induced spin echo is a refocusing phenomenon caused by the control pulse, where the macroscopic signal, after disappearing, revives from the sustained sublevel coherences when the optical excitation, the control pulse, is applied.

In order to investigate the effect of the control pulse, we consider an ensemble of three-level atoms whose ground state is a degenerated doublet, $|1'\rangle$ and $|2'\rangle$, and excited state is $|3\rangle$. The Hamiltonian of the system is given by

$$\mathcal{H} = \mathcal{H}_0 + \mathcal{H}_1 + \mathcal{H}_2, \tag{1}$$

where $\mathcal{H}_0$ is the three-level atomic Hamiltonian, $\mathcal{H}_1$ is a time-independent perturbation such as the Zeeman interaction, and $\mathcal{H}_2$ is the atom-light interaction. The density matrix ρ' for the unperturbed Hamiltonian $\mathcal{H}_0$ and ρ for the per-

turbed Hamiltonian $\mathcal{H}_0+\mathcal{H}_1$ are transformed by the relation $\rho=T\rho' T^{-1}$, where

$$T=\begin{pmatrix} \cos\frac{\theta}{2} & -\sin\frac{\theta}{2} \\ \sin\frac{\theta}{2} & \cos\frac{\theta}{2} \end{pmatrix}. \tag{2}$$

The frequency difference ω_{21} between $|1\rangle$ and $|2\rangle$ is $(E_2-E_1)/\hbar$, where E_1 and E_2 are their eigenvalues. The sublevel splitting ω_{21} is inhomogeneously distributed.

The atoms are excited by light pulses at $t=0$ and τ. The electric fields of the excitation pulses are assumed to have rectangular envelopes. Any element of the density matrix after the light excitation is expressed by a linear combination of the elements before the light excitation [46]. In the case of the control pulse, here, $\rho_{jk}(\tau')=\Sigma_{ab}c_{jk}^{ab}\rho_{ab}(\tau)$, where τ and τ' are the times at the beginning and the end of the control pulse, respectively, and c_{jk}^{ab} are the coefficients that connect the matrix elements of $\rho(\tau)$ to those of $\rho(\tau')$ in the perturbed system.

The signal $S(t)$ of the sublevel coherence is proportional to the ensemble average $\langle\exp(-i\omega_{21}t)\tilde{\rho}_{21}(t)\rangle$, and that after the control pulse is derived to [47]

$$S(t)\propto c_{21}^{12}\langle\exp[-i\omega_{21}(t-\tau-\tau')]\tilde{\rho}_{12}(\tau)\rangle+c_{21}^{21}\langle\exp[-i\omega_{21}(t+\tau-\tau')]\tilde{\rho}_{21}(\tau)\rangle+\langle\exp[-i\omega_{21}(t-\tau')]\sum_a c_{21}^{aa}\tilde{\rho}_{aa}(\tau)\rangle, \tag{3}$$

where $\rho_{ab}(t)=\tilde{\rho}_{ab}(t)\exp(-i\omega_{ab}t)$, and $\tilde{\rho}_{ab}$ represents the slowly varying factor of ρ_{ab}. The first term is the echo signal that has a nonzero value at $t=\tau+\tau'\simeq 2\tau$ when the width of the control pulse $t_p=\tau'-\tau$ is much smaller than τ. The refocusing efficiency of the optically induced spin echo is obtained from the coefficient c_{21}^{12}. The second and third terms are the FID signals of the generation and control pulses, respectively.

Next, we consider the time evolution of the density matrix during the control pulse and derive the expression of the refocusing efficiency. During the light pulse, the perturbation Hamiltonian $\mathcal{H}_2$ is added to $\mathcal{H}$. In the case of the impact excitation, where the condition $\omega_{21}t_p\ll 1$ is satisfied, the perturbation Hamiltonian $\mathcal{H}_1$ can be neglected during the light pulse. Using the rotating-wave approximation, the total Hamiltonian $\mathcal{H}_0+\mathcal{H}_2$ during the light pulse results in the Hamiltonian $\mathcal{H}_r$ in the rotating frame,

$$\mathcal{H}_r=\hbar\Delta|3\rangle\langle 3|+\frac{\hbar\chi}{2}(|1'\rangle\langle 3|+|3\rangle\langle 1'|), \tag{4}$$

where $\Delta=\omega_{31}-\omega$ represents the detuning of the laser frequency ω from the resonance frequency ω_{31} of the optical transition.

The equations of motion for this system are given by the following set of differential equations:

$$\frac{d}{dt}\rho'_{11}=\frac{i\chi}{2}(\rho'_{13}-\rho'_{31})+\gamma_1(\rho'_{11}-\rho'_{22})+\frac{\Gamma_1}{2}\rho'_{33},$$

$$\frac{d}{dt}\rho'_{12}=-\frac{i\chi}{2}\rho'_{32}-\gamma_2\rho'_{12},$$

$$\frac{d}{dt}\rho'_{13}=\frac{i\chi}{2}(\rho'_{11}-\rho'_{33})+(i\Delta-\Gamma_2)\rho'_{13},$$

$$\frac{d}{dt}\rho'_{21}=\frac{i\chi}{2}\rho'_{23}-\gamma_2\rho'_{21},$$

$$\frac{d}{dt}\rho'_{22}=-\gamma_1(\rho'_{11}-\rho'_{22})+\frac{\Gamma_1}{2}\rho'_{33},$$

$$\frac{d}{dt}\rho'_{23}=\frac{i\chi}{2}\rho'_{21}+(i\Delta-\Gamma_2)\rho'_{23},$$

$$\frac{d}{dt}\rho'_{31}=-\frac{i\chi}{2}(\rho'_{11}-\rho'_{33})+(-i\Delta-\Gamma_2)\rho'_{31},$$

$$\frac{d}{dt}\rho'_{32}=-\frac{i\chi}{2}\rho'_{12}+(-i\Delta-\Gamma_2)\rho'_{32},$$

$$\frac{d}{dt}\rho'_{33}=-\frac{i\chi}{2}(\rho'_{13}-\rho'_{31})-\Gamma_1\rho'_{33}, \tag{5}$$

where ρ' is the density matrix in the rotating frame; Γ_1, the optical population decay rate; and Γ_2, the optical dephasing rate. In addition, we assume the sublevel decay rate γ_1 and the dephasing rate γ_2 between the ground-state levels $|1'\rangle$ and $|2'\rangle$. For free atoms, the optical dephasing rate is given by $\Gamma_2=\Gamma_1/2$. Since the optical relaxation rates Γ_1 and Γ_2 are much larger than χ, γ_1, and γ_2, a stationary state of the optical elements of the density matrix, which are related to the excited state and the optical coherence, is attained very quickly after turning on the light, so that five of the equations given in Eq. (5) fulfill the steady-state conditions,

$$\frac{d}{dt}\rho'_{13}=\frac{d}{dt}\rho'_{23}=\frac{d}{dt}\rho'_{31}=\frac{d}{dt}\rho'_{32}=\frac{d}{dt}\rho'_{33}=0. \tag{6}$$

This allows us to eliminate the optical elements of the density matrix from the set of Eqs. (5). This procedure is called the adiabatic elimination of the optical coherence [48]. Then, we obtain differential equations for the population and sublevel coherence in the ground state,

$$\frac{d}{dt}\rho'_{11}=-\frac{\chi^2\Gamma_2}{4\Delta^2+\chi^2+4\Gamma_2^2}\rho'_{11},$$

$$\frac{d}{dt}\rho'_{12}=\frac{i\chi^2}{4(\Delta-i\Gamma_2)}\rho'_{12},$$

$$\frac{d}{dt}\rho'_{21}=-\frac{i\chi^2}{4(\Delta+i\Gamma_2)}\rho'_{21},$$

$$\frac{d}{dt}\rho'_{22} = \frac{\chi^2\Gamma_2}{4\Delta^2+\chi^2+4\Gamma_2^2}\rho'_{11}, \tag{7}$$

where γ_1 and γ_2 are neglected, and the time evolution of the sublevel coherence during the control pulse is ignored.

The elements $\rho'_{ab}(\tau')$ of the density matrix at the end of the control pulse are derived from the differential equations in Eqs. (7). The refocusing efficiency c_{21}^{12} of the optically induced spin echoes in Eq. (3) can be derived from the relation between $\rho_{21}(\tau')$ and $\rho_{ab}(\tau)$ in the perturbed system, and is given by

$$c_{21}^{12} = \left[\exp\left(-\frac{\chi^2\Gamma_2 t_p}{4\Delta^2+\chi^2+4\Gamma_2^2}\right) - \cos\left(\frac{\Delta\chi^2 t_p}{4(\Delta^2+\Gamma_2^2)}\right) \times \exp\left(-\frac{\chi^2\Gamma_2 t_p}{4(\Delta^2+\Gamma_2^2)}\right)\right] 2\sin^2\frac{\theta}{2}\cos^2\frac{\theta}{2}, \tag{8}$$

where $t_p=\tau'-\tau$ is the duration of the control pulse.

In the previous theory [45], the refocusing efficiency becomes zero for the on-resonant excitation $\Delta=0$. This is because the optically induced spin echoes for the on-resonant manipulation are not considered in that theory. In our theory, on the other hand, the optically induced spin echoes for the on-resonant manipulation are also included. Substituting zero for Δ in Eq. (8), the refocusing efficiency for the on-resonant manipulation is given by

$$c_{21}^{12} = \left[\exp\left(-\frac{\alpha\Gamma_2 t_p}{\alpha+4\Gamma_2}\right) - \exp\left(-\frac{\alpha t_p}{4}\right)\right] 2\sin^2\frac{\theta}{2}\cos^2\frac{\theta}{2}, \tag{9}$$

where $2\alpha=2\chi^2/\Gamma_2$ is the optical pumping rate. In the limiting case $\alpha \ll \Gamma_2, 1/t_p$, Eq. (9) is rewritten as

$$c_{21}^{12} \simeq \frac{\alpha^2 t_p}{8\Gamma_2}\sin^2\frac{\theta}{2}\cos^2\frac{\theta}{2}, \tag{10}$$

which implies that the refocusing efficiency is proportional to the square of the light intensity in the low-intensity limit. This proportionality is consistent with the result of the theory for the on-resonant manipulation [47].

III. EXPERIMENT

We performed two types of optically induced spin-echo experiments, on-resonant manipulation and off-resonant manipulation, where the excitation by the control pulse is on- and off-resonant. The pump and probe of the optically induced magnetization for the (a) on- and (b) off-resonant manipulations are schematically shown in Fig. 2.

The amplitude of the optically induced spin-echo signal is detected by the optical means. The time evolution of the magnetization is monitored by a polarimeter as the change in the polarization of the linearly polarized probe pulse [49]. The polarimeter can separately detect the signal due to the magnetic circular dichroism (MCD) or that due to the magnetic circular birefringence (MCB) where a quarter-wave plate is in or out. The spectra of MCD and MCB are related by the Kramers-Kronig relations [50]. MCD and MCB,

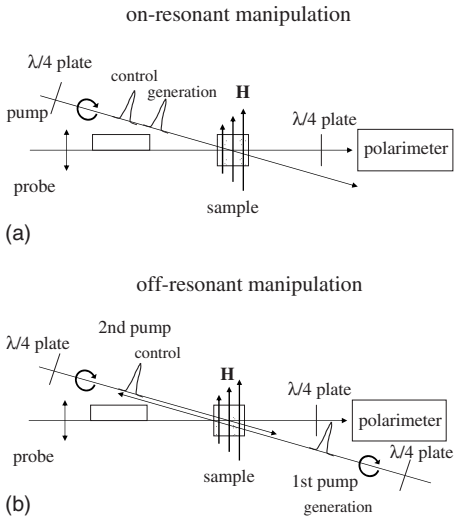

FIG. 2. Pump and probe of the optically induced magnetization for the (a) on- and (b) off-resonant manipulations.

which generally coexist, are distinguished completely by the polarimeter. MCD detection is used both for the on- and off-resonant manipulations of the optically induced spin echoes. The signal detected by the polarimeter includes information about the phase of magnetization. The magnetization induced by σ^+ and σ^- polarized pump pulses have opposite directions, and the probed signals detected by the polarimeter have opposite signs.

The spin system in our experiment is the Zeeman sublevels of the $S_{1/2}$ ground state of rubidium atoms. The D_1 line ($\lambda=794.8$ nm) is used for the optical excitation. The generation and control pulses are provided by an acousto-optic modulator (AOM) from the continuous output of a Ti:sapphire laser or a laser diode, and are circularly polarized by a $\lambda/4$ plate. The probe pulse is provided by another AOM from the output of the Ti:sapphire laser. The pulse widths of the pump and probe pulses are ~ 1 μs and ~ 5 ms. The rubidium vapor is confined in a 1-cm cell with helium buffer gas at a pressure of ~ 5 Torr. The diameter of the beams at the sample is approximately 1 mm, and the angle between the two beams is less than 1°.

In order to shorten the decay time of the FID signals, a spatially and temporally inhomogeneous magnetic field is applied. The spatial inhomogeneity is created by an electromagnet that gives the gradient of the magnetic field, and the temporal inhomogeneity is created by a multistable magnetic field whose values have a Gaussian distribution. Its clock time is longer than the time of the pulse sequence for the spin echoes.

In the experiment of the on-resonant manipulation, a Ti:sapphire laser is used. The scheme of the pump and probe is shown in Fig. 2(a). The laser beam is divided into the pump light and the probe light by a beam splitter. Then, the generation, control, and probe pulses have the same frequency. The generation pulse creates the magnetization, and the control pulse rephases the spins dephased by the inhomogeneous magnetic field.

In the experiment of the off-resonant manipulation with two lasers, a Ti:sapphire laser and a laser diode are used. The

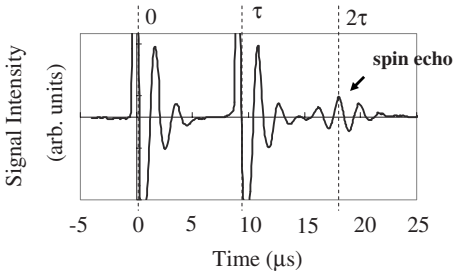

FIG. 3. Typical experimental result of the observed spin transients.

scheme of the pump and probe is shown in Fig. 2(b). The generation and probe pulses are provided by the laser diode, whose frequency is tuned to the resonance line of ^{87}Rb ($F=2\rightarrow F'=1$), where F and F' are the total angular momenta including the nucleus in the ground and excited states, respectively. With regard to the resonance, the generation efficiency of the magnetization and the probe efficiency for the MCD detection increase. The control pulse is provided by the Ti:sapphire laser. Its frequency is changed around the resonance line to examine the effect of the spin manipulation.

IV. RESULTS

A typical experimental result of the observed spin transients is shown in Fig. 3. The spin-echo signal appears at $t=2\tau$ when the generation and control pulses are applied at $t=0$ and τ, which is the same as the spin echoes in the magnetic resonance, the nuclear magnetic resonance or the electron spin resonance.

A. FID

As seen in Fig. 3, the FID signals appear after the generation and control pulses, which are due to the Larmor precession of the optically induced magnetization around the magnetic field. The magnetic-field dependence of the FID signal in the ground state of ^{87}Rb is shown in Fig. 4(a), where the pump and probe pulses are tuned to the transition of ^{87}Rb ($F=2\rightarrow F'=1$) and the inhomogeneous field is not applied. The signal for zero external field is the FID signal in the residual magnetic field at the Rb cell. The decay time of 3 μs is determined by the transit time across the laser beam. The Fourier transform of the FID signals shown in Fig. 4(a) is shown in Fig. 4(b).

The Larmor frequency increases with the magnetic field. The proportional constant of the frequency to the magnetic field is 0.7 MHz/Oe, which corresponds to the effective g factor in the ground state.

The frequency dependence of the signal intensity of the observed FID is shown in Fig. 5. The probe pulse is tuned to the transition of ^{87}Rb ($F=2\rightarrow F'=1$), and the frequency of the pump pulse is changed to examine the excitation frequency dependence. The solid circles show the observed signal intensity. The transmitted intensity of the pump pulse for a reference cell is shown to indicate the positions of the absorption lines. The signal intensity has a peak at the

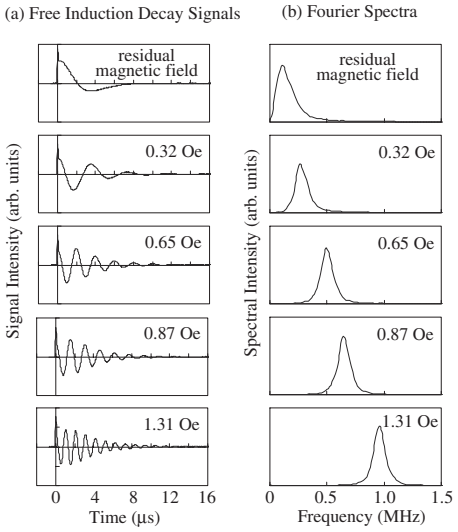

FIG. 4. (a) Magnetic-field dependence of the observed free induction decay signals in the ground state of ^{87}Rb. (b) Fourier transform of the free induction decay signals in (a).

probed line. Another peak appears in the higher frequency side because the lower state (^{87}Rb, $F=2$), is common to the probed line ($F=2\rightarrow F'=1$) and the neighboring line ($F=2\rightarrow F'=2$).

B. Spin echoes

The frequency dependence of the signal intensity of the optically induced spin echoes observed for the on-resonant manipulation is shown in Fig. 6. The generation, control, and probe pulses are provided by a single laser, and their frequency is swept simultaneously in the inhomogeneous magnetic field. The solid circles show the signal intensity of the observed spin echoes. The transmitted intensity for a reference cell is also shown to indicate the positions of the absorption lines. The spin-echo signal appears around each absorption peak.

The frequency dependence of the signal intensity of the optically induced spin echoes observed for the off-resonant

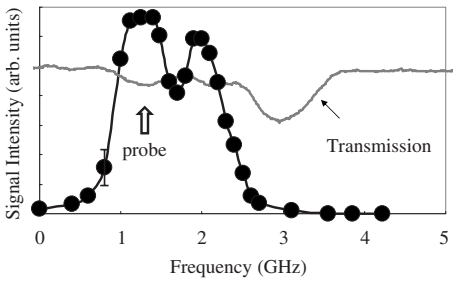

FIG. 5. Frequency dependence of the signal intensity of the observed FID. The probe pulse is tuned to the ^{87}Rb ($F=2\rightarrow F'=1$) line, and the frequency of the pump pulse is changed. The solid circles show the observed signal intensity. The solid curve serves as a visual guide. The transmitted intensity of the pump pulse for a reference cell is also shown. A characteristic error bar is shown on one of the observed data, which is determined by the stability of the laser frequency and the electrical noise of the detection system.

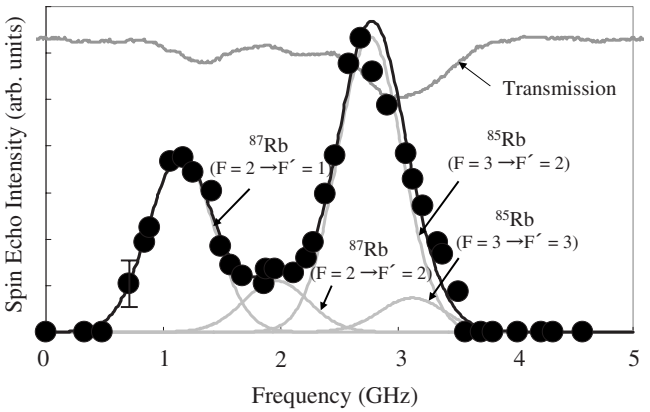

FIG. 6. Frequency dependence of the signal intensity of the optically induced spin echoes observed for the on-resonant manipulation. The generation, control, and probe pulses are provided by a single laser, and their frequency is swept simultaneously. The solid circles show the signal intensity of the observed spin echoes. The black solid line shows the calculated curve obtained from the sum of the contributions from the four transition lines. The transmitted intensity for a reference cell is also shown. A characteristic error bar is shown on one of the observed data, which is determined by the stability of the laser frequency and the electrical noise of the detection system.

excitation is shown in Fig. 7. The frequencies of the generation and probe pulses, which are provided by the laser diode, are tuned to the resonance line of ^{87}Rb ($F=2\rightarrow F'=1$). Only the frequency of the control pulse, which is provided by the Ti:sapphire laser, is changed. The solid circles show the signal intensity of the observed spin echoes. The transmitted intensity for a reference cell is also shown to indicate the positions of the absorption lines. The spin-echo signal at the probed line does not have a large intensity. The signal, in

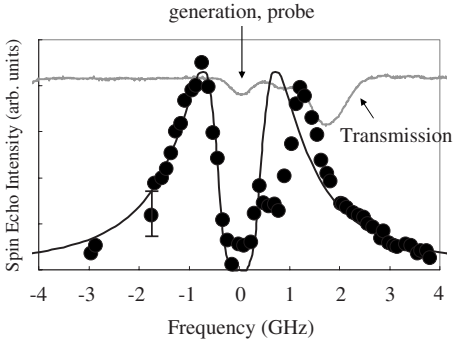

FIG. 7. Frequency dependence of the signal intensity of the optically induced spin echoes observed for the off-resonant manipulation. The generation and probe pulses are provided by a laser diode, which is tuned to the ^{87}Rb ($F=2\rightarrow F'=1$) line. The control pulse is provided by a Ti:sapphire laser, and its frequency is changed. The solid circles show the signal intensity of the observed spin echoes. The solid curve shows the theoretical frequency dependence of the spin-echo intensity obtained from Eq. (8). The transmitted intensity for a reference cell is also shown. A characteristic error bar is shown on one of the observed data, which is determined by the stability of the laser frequency and the electrical noise of the detection system.

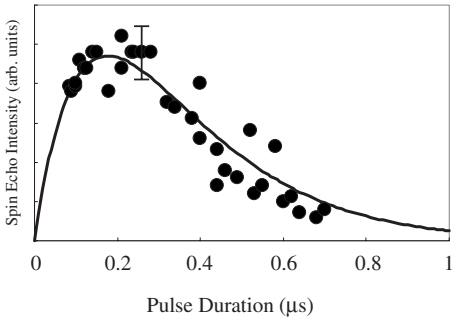

FIG. 8. Dependence of the spin-echo intensity on the control pulse duration for the on-resonant manipulation. The solid circles show the observed spin-echo intensity. The solid curve shows the theoretical pulse-duration dependence of the spin-echo intensity obtained from Eq. (8). A characteristic error bar is shown on one of the observed data, which is determined by the stability of the laser frequency and the electrical noise of the detection system.

contrast with the on-resonant case, has a large intensity at the off-resonant wings of the probed line.

The pulse-duration dependences of the spin-echo intensity for the on- and off-resonant manipulations are shown in Figs. 8 and 9, respectively. The detuning Δ is zero for the on-resonant manipulation and approximately 5 GHz for the off-resonant manipulation, and the duration of the control pulse is changed. The pulse-duration dependence for the on-resonant manipulation in Fig. 8 exhibits a monotonously decreasing intensity after the maximum value, while that for the off-resonant manipulation in Fig. 9 exhibits an oscillating behavior.

V. DISCUSSION

In the process of the production of spin echoes by optical means, the generation pulse creates polarized spins or magnetization, and the control pulse manipulates the phase of the spins. The optically induced spin-echo signal results from the refocusing of the dephased spins in the inhomogeneous magnetic field after the control pulse.

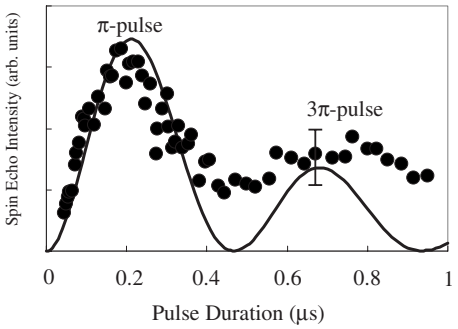

FIG. 9. Dependence of the spin-echo intensity on the control pulse duration for the off-resonant manipulation. The solid circles show the observed spin-echo intensity. The solid curve shows the theoretical pulse-duration dependence of the spin-echo intensity obtained from Eq. (8). A characteristic error bar is shown on one of the observed data, which is determined by the stability of the laser frequency and the electrical noise of the detection system.

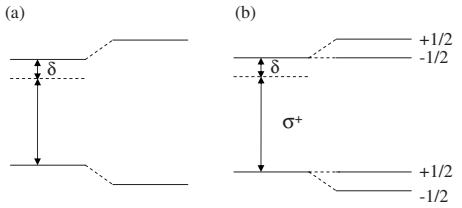

FIG. 10. Schematic diagram for the light shift. (a) Energy shift in a two-level system interacting with an off-resonant light field. (b) Energy splitting in a $\mathbf{J}=1/2$ $\mathbf{J}'=1/2$ system interacting with a circularly polarized light field, for example σ^+ light.

The refocusing mechanism caused by the control pulse for the off-resonant manipulation is different from that for the on-resonant manipulation. The refocusing mechanism for the on-resonant manipulation is due to the optical pumping. That for the off-resonant manipulation, on the other hand, is due to the light shift [51]. The light shift caused by the circularly polarized light makes a fictitious magnetic field in the laser-beam direction since the degeneracy appears to be lifted, as shown in Fig. 10. From the viewpoint of spin manipulation, the off-resonant manipulation is more convenient than the on-resonant one because the former does not change the population.

A. Vector models

We consider vector models for the optically induced spin echoes for both the on-resonant and off-resonant manipulations, which are shown in Figs. 11 and 12, respectively. Each

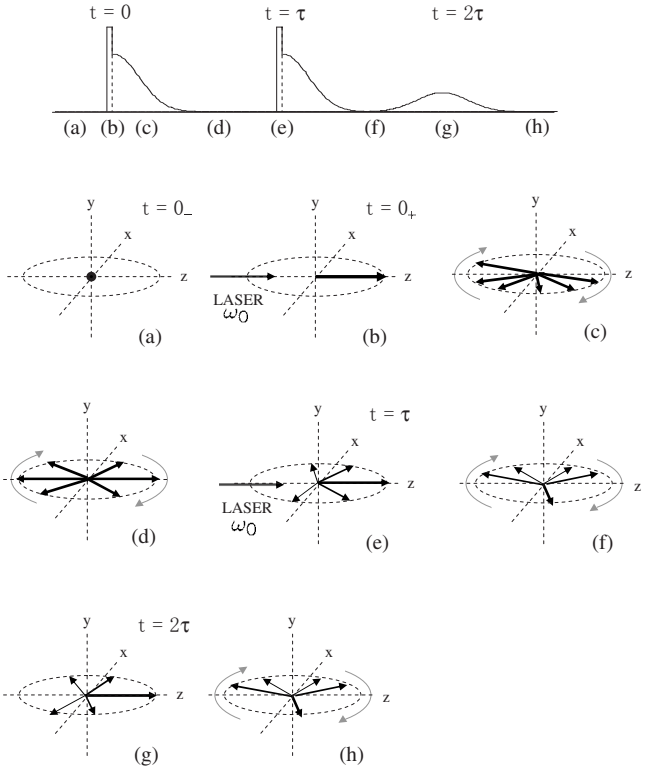

FIG. 11. Vector model for the optically induced spin echoes for the on-resonant manipulation.

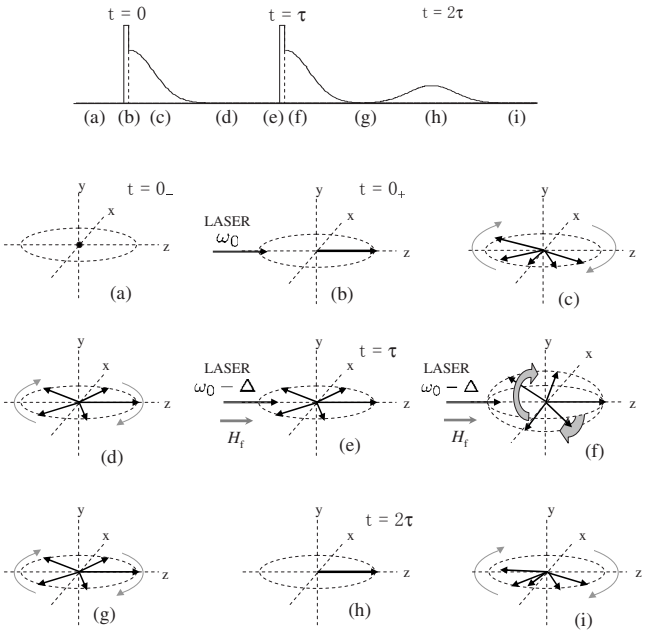

FIG. 12. Vector model for the optically induced spin echoes for the off-resonant manipulation.

vector model is given under the following assumptions. (1) The lifetime of the excited state is very short as compared to the dephasing time of the coherence in the ground state. (2) There is no magnetization in the thermal equilibrium. (3) The laser pulses propagate along the z axis, and an inhomogeneous magnetic field is applied along the y axis. (4) The spin motion is considered in the laboratory frame.

In each vector model, the generation pulse applied at $t=0$ is used to create a spin polarization or the optically induced magnetization along the $+z$ axis [52]. After the generation pulse, different spins precess at different Larmor frequencies Ω_L because of the inhomogeneous distribution of the magnetic field. Therefore, the macroscopic spin polarization disappears in the appearance. The operation of the control pulse is different between the on- and off-resonant manipulations.

In the case of the on-resonant manipulation, the control pulse tuned to the resonance line is applied at $t=\tau$. The sublevels in the ground state are selectively depopulated by the optical pumping with a circularly polarized pulse. The control pulse has an effect to remove the left directing spins, whose z component is negative, more than the right directing spins, whose z component is positive, as shown in Fig. 11(e). The right directing spins at $t=\tau$ have an angular velocity of $\sim 2\pi n/\tau$ (n is a integer). After the control pulse, the spins are dephased again in the inhomogeneous magnetic field. At $t=2\tau$ after the free precession for an additional time τ, however, the spins refocus in the $+z$ direction, as shown in Fig. 11(g), where the right directing spins are more than the left directing spins. This is the spin-echo signal.

In the case of the off-resonant manipulation, the control pulse is detuned from the resonance line to which the generation pulse is tuned, and creates a fictitious magnetic field caused by the light shift. The spins are turned around the z axis, as shown in Fig. 12(f). For an appropriate pulse dura-

tion, a π pulse can be realized, where the spins rotate by 180° around the z axis. This operation of the control pulse is similar to that in the magnetic resonance, and the spin-echo signals appear at $t=2\tau$.

B. Frequency dependence

The observed frequency dependence of the signal intensity of the optically induced spin echoes for the on-resonant manipulation shown in Fig. 6 can be explained by considering that the frequency dependence is the sum of the contributions from different transition lines and that each contribution has an absorption line shape. The solid curve shown in Fig. 6 is the calculated curve obtained from the sum of the Doppler-broadened Gaussian line shapes and it suitably explains the observed frequency dependence. The lines, whose total-angular-momentum number F in the ground state is lager than that (F') in the excited state, contribute significantly to the spin-echo signal. This can be explained as follows. For $F<F'$, all sublevels in the ground state are depopulated according to the selection rules for the pump polarization. The effect of hyperfine pumping decreases the population and the population difference in the ground state. For $F>F'$, on the other hand, some sublevels are not depopulated, and a large population difference is created. The case for $F=F'$ is an intermediate case.

The solid curve shown in Fig. 7 indicated the theoretical frequency dependence of the signal intensity of the optically induced spin echoes for the off-resonant manipulation, which is obtained from Eq. (8). The fitting parameters are $t_p=100$ ns, $\Gamma_2=2\pi\times 150$ MHz, and $\chi=2\pi\times 105$ MHz. These values are consistent with the experimental values. The value of Γ_1, which is broader than the natural width, is explained by the power broadening. The theoretical curve suitably explains the observed frequency dependence. The deviation of the observed intensity from the theoretical curve around the neighboring absorption line ^{87}Rb $(F=2\rightarrow F'=2)$ in the higher frequency side is considered to be caused by the effect of the optical pumping, because the excited line ^{87}Rb $(F=2\rightarrow F'=1)$ by the generation pulse and the neighboring line have the same lower level. The signals around the excited absorption line are due to the spin echoes for the on-resonant manipulation. Figure 7 shows that the signal intensity of the spin echoes for the off-resonant manipulation has a maxima on both the higher- and lower-frequency sides of the relevant absorption line and is much larger than that for the on-resonant manipulation in this experiment.

C. Dependence on the control pulse duration

The solid curves shown in Figs. 8 and 9 indicate the theoretical dependences of the spin-echo intensity on the control pulse duration for the on- and off-resonant manipulations, respectively, which are obtained from Eq. (8). The fitting parameters in Fig. 8 are $\Delta=0$, $\Gamma_2=2\pi\times 17$ MHz, and $\chi=2\pi\times 8$ MHz. The theoretical curve suitably explains the observed pulse-duration dependence. The fitting parameters in Fig. 9 are $\Delta=2\pi\times 0.8$ GHz, $\Gamma_2=2\pi\times 120$ MHz, and $\chi=2\pi\times 82$ MHz. The theoretically predicted oscillating behavior is observed in the experiment. The observed amplitude of the oscillation, however, is smaller than the expected one. This may be caused by the spatial distribution of χ, which is proportional to the electric-field amplitude of the laser beam.

The spin-echo intensity for the off-resonant manipulation has peak values when the control pulse rotates the spins by $(2n+1)\pi$, where n is an integer. This is easily understood from the vector model for the off-resonant manipulation shown in Fig. 12. The first and second peaks in Fig. 9 correspond to the π pulse and 3π pulse of the control light, respectively.

In the off-resonant manipulation, the rotation axis is determined by the direction of the control pulse. The rotation angle can be adjusted by the intensity or duration of the control pulse. The off-resonant manipulation gives the possibility of arbitrary-angle spin rotation around an arbitrary axis.

VI. SUMMARY

Two types of optically induced spin echoes, whose refocusing mechanisms due to the control pulse are different, were studied theoretically and experimentally. The off-resonant type of spin echoes is created by the effect of the light shift, while the on-resonant type is created by the effect of the optical pumping. Vector models for the two types of spin echoes were presented. A theory of the optically induced spin echoes was considered, and the general expression for the refocusing efficiency of the control pulse, which can be applied to both types of spin echoes, was derived by using the density matrix.

The optically induced FID and spin echoes in rubidium atoms were observed by using the polarization spectroscopy with the pump-probe technique. Two types of spin echoes, on- and off-resonant manipulations, were observed, and the frequency and duration dependences of the control pulse were examined. The observed frequency dependences of the FID signal and the spin-echo signal for the on-resonant manipulation can be explained by the simple sum of the contributions from the absorption lines. The observed frequency dependence of the spin-echo signal exhibits a large intensity at the off-resonant wings of the probed line. The observed duration dependence for the off-resonant manipulation exhibits an oscillating behavior, while that for the on-resonant manipulation exhibits a monotonously decreasing intensity after the maximum value. The observed frequency and duration dependences are suitably explained by our theory of the optically induced spin echoes. In our experiment, the observed signal intensity of the spin echoes for the off-resonant manipulation on the higher- and lower-frequency sides of the absorption line is much larger than that for the on-resonant manipulation on the absorption line.

From the viewpoint of spin manipulation, the off-resonant manipulation is more convenient than the on-resonant one, because the former manipulation does not change the population. The off-resonant manipulation gives the possibility of arbitrary-angle spin rotation around an arbitrary axis.

ACKNOWLEDGMENTS

We would like to thank K. Konishi, Y. Onizuka, and D. Nomoto for experimental help in the earlier stage of the present experiment.

[1] J. I. Cirac and P. Zoller, Phys. Rev. Lett. **74**, 4091 (1995).
[2] C. Monroe, Nature (London) **416**, 238 (2002).
[3] C. Monroe, D. M. Meekhof, B. E. King, S. R. Jefferts, W. M. Itano, D. J. Wineland, and P. Gould, Phys. Rev. Lett. **75**, 4011 (1995).
[4] C. Monroe, D. M. Meekhof, B. E. King, W. M. Itano, and D. J. Wineland, Phys. Rev. Lett. **75**, 4714 (1995).
[5] C. A. Sackett, D. Kielpinski, B. E. King, C. Langer, V. Meyer, C. J. Myatt, M. Rowe, Q. A. Turchette, W. M. Itano, D. J. Wineland, and C. Monroe, Nature (London) **404**, 256 (2000).
[6] B. Julsgaard, A. Kozhekin, and E. S. Polzik, Nature (London) **413**, 400 (2001).
[7] R. Dumke, M. Volk, T. Müther, F. B. J. Buchkremer, G. Birkl, and W. Ertmer, Phys. Rev. Lett. **89**, 097903 (2002).
[8] D. Schrader, I. Dotsenko, M. Khudaverdyan, Y. Miroshnychenko, A. Rauschenbeutel, and D. Meschede, Phys. Rev. Lett. **93**, 150501 (2004).
[9] H. Yuan and S. Lloyd, Phys. Rev. A **75**, 052331 (2007).
[10] L. You and M. S. Chapman, Phys. Rev. A **62**, 052302 (2000).
[11] T. Nakanishi, K. Yamane, and M. Kitano, Phys. Rev. A **65**, 013404 (2001).
[12] V. Meyer, M. A. Rowe, D. Kielpinski, C. A. Sackett, W. M. Itano, C. Monroe, and D. J. Wineland, Phys. Rev. Lett. **86**, 5870 (2001).
[13] S. Massar and E. S. Polzik, Phys. Rev. Lett. **91**, 060401 (2003).
[14] D. Leibfried, B. DeMarco, V. Meyer, D. Lucas, M. Barrett, J. Britton, W. M. Itano, B. Jelenkovic, C. Langer, T. Rosenband, and D. J. Wineland, Nature (London) **422**, 412 (2003).
[15] S. Braungardt, A. Sen (De), U. Sen, and M. Lewenstein, Phys. Rev. A **76**, 042307 (2007).
[16] M. J. McDonnell, J.-P. Stacey, S. C. Webster, J. P. Home, A. Ramos, D. M. Lucas, D. N. Stacey, and A. M. Steane, Phys. Rev. Lett. **93**, 153601 (2004).
[17] I. D'Amico, B. W. Lovett, and T. P. Spiller, Phys. Rev. A **76**, 030302(R) (2007).
[18] M. P. A. Jones, J. Beugnon, A. Gaëtan, J. Zhang, G. Messin, A. Browaeys, and P. Grangier, Phys. Rev. A **75**, 040301(R) (2007).
[19] T. Gaebel, M. Domhan, I. Popa, C. Wittmann, P. Neumann, F. Jelezko, J. R. Rabeau, N. Stavrias, A. D. Greentree, S. Prawer, J. Meijer, J. Twamley, P. R. Hemmer, and J. Wrachtrup, Nat. Phys. **2**, 408 (2006).
[20] A. M. Zagoskin, J. R. Johansson, S. Ashhab, and Franco Nori, Phys. Rev. B **76**, 014122 (2007).
[21] X. Q. Li, C. Y. Hu, L. X. Cen, H. Z. Zheng, and Y. J. Yan, Phys. Rev. B **66**, 235207 (2002).
[22] M. V. Berry, Proc. R. Soc. London, Ser. A **392**, 45 (1984).
[23] Y. Aharonov and J. Anandan, Phys. Rev. Lett. **58**, 1593 (1987).
[24] G. Delacretaz, E. R. Grant, R. L. Whetten, L. Woste, and J. W. Zwanziger, Phys. Rev. Lett. **56**, 2598 (1986).
[25] R. Y. Chiao and Y. S. Wu, Phys. Rev. Lett. **57**, 933 (1986); T. Tomita and R. Y. Chiao, *ibid.* **57**, 937 (1986).
[26] R. Tycko, Phys. Rev. Lett. **58**, 2281 (1987).
[27] D. Suter, G. Chingas, R. A. Harris, and A. Pines, Mol. Phys. **61**, 1327 (1987).
[28] D. Suter, K. T. Mueller, and A. Pines, Phys. Rev. Lett. **60**, 1218 (1988).
[29] T. Bitter and D. Dubbers, Phys. Rev. Lett. **59**, 251 (1987).
[30] L. M. K. Vandersypen, M. Steffen, G. Breyta, C. S. Yannoni, M. H. Sherwood, and I. L. Chuang, Nature (London) **414**, 883 (2001).
[31] L. M. K. Vandersypen and I. L. Chuang, Rev. Mod. Phys. **76**, 1037 (2005).
[32] S. Furue, T. Kohmoto, M. Kunitomo, and Y. Fukuda, Phys. Lett. A **345**, 415 (2005).
[33] Q. Zhang, A. V. Nurmikko, A. Anguelouch, G. Xiao, and A. Gupta, Phys. Rev. Lett. **89**, 177402 (2002).
[34] J. A. Gupta, R. Knobel, N. Samarth, and D. D. Awschalom, Science **292**, 2458 (2001).
[35] A. Greilich, R. Oulton, E. A. Zhukov, I. A. Yugova, D. R. Yakovlev, M. Bayer, A. Shabaev, Al. L. Efros, I. A. Merkulov, V. Stavarache, D. Reuter, and A. Wieck, Phys. Rev. Lett. **96**, 227401 (2006).
[36] Y. Wu, E. D. Kim, X. Xu, J. Cheng, D. G. Steel, A. S. Bracker, D. Gammon, S. E. Economou, and L. J. Sham, Phys. Rev. Lett. **99**, 097402 (2007).
[37] Th. Gerrits, H. A. M. van den Berg, J. Hohlfeld, L. Bär, and Th. Rasing, Nature (London) **418**, 509 (2002).
[38] F. Hansteen, A. Kimel, A. Kirilyuk, and T. Rasing, Phys. Rev. Lett. **95**, 047402 (2005).
[39] C. D. Stanciu, F. Hansteen, A. V. Kimel, A. Tsukamoto, A. Itoh, A. Kirilyuk, and Th. Rasing, Phys. Rev. Lett. **98**, 207401 (2007).
[40] C. D. Stanciu, F. Hansteen, A. V. Kimel, A. Kirilyuk, A. Tsukamoto, A. Itoh, and Th. Rasing, Phys. Rev. Lett. **99**, 047601 (2007).
[41] R. C. Myers, M. H. Mikkelsen, J.-M. Tang, A. C. Gossard, M. E. Flatte, and D. D. Awschalom, Nat. Mater. **7**, 203 (2008).
[42] N. A. Kurnit, I. D. Abella, and S. R. Hartmann, Phys. Rev. Lett. **13**, 567 (1964).
[43] J. P. Gordon and C. H. Wang, Phys. Rev. **179**, 294 (1969).
[44] Y. Fukuda, K. Yamada, and T. Hashi, Opt. Commun. **44**, 297 (1983).
[45] M. Rosatzin, D. Suter, and J. Mlynek, Phys. Rev. A **42**, 1839 (1990).
[46] M. Tanigawa, Y. Fukuda, M. Kunitomo, T. Hashi, and M. Mishina, J. Opt. Soc. Am. B **9**, 313 (1992).
[47] T. Mishina, M. Tanigawa, Y. Fukuda, and, T. Hashi, Opt. Com-

mun. **62**, 166 (1987).
[48] D. Suter and J. Mlynek, in *Advances in Magnetic and Optical Resonance*, edited by W. S. Warren (Academic, New York, 1991), Vol. 16, p. 1.
[49] T. Kohmoto, Y. Fukuda, M. Kunitomo, and K. Isoda, Phys. Rev. B **62**, 579 (2000).
[50] C. Kittel and P. L. McEuen, *Introduction to Solid State Physics*, 8th ed. (Wiley, Hoboken, 2005).
[51] B. S. Mathur, H. Tang, and W. Happer, Phys. Rev. **171**, 11 (1968).
[52] D. Suter, M. Rosatzin, and J. Mlynek, Phys. Rev. A **41**, 1634 (1990).